SAPIENZA
UNIVERSITÀ DI ROMA

Modeling and motion analysis of autonomous paragliders

Chiara Toglia
Marilena Vendittelli

Technical Report n. 5, 2010

Modeling and motion analysis of autonomous paragliders

Chiara Toglia   Marilena Vendittelli *

Abstract

This report describes a preliminary study on modeling and control of parafoil and payload systems with the twofold objective of developing tools for automatic testing and classification of parafoils and of devising autonomous paragliders able to accomplish long-range delivery or monitoring tasks. Three different models of decreasing complexity are derived and their accuracy compared by simulation.

Keywords: autonomous aerial vehicles, modeling, aerodynamics.

---

*C. Toglia and M. Vendittelli are with the Dipartimento di Informatica e Sistemistica, Università di Roma "La Sapienza", Via Ariosto 25, 00185 Roma, Italy. E-mail: {toglia,venditt}@dis.uniroma1.it

1 Introduction

This report describes the ongoing research on modeling and control of paragliders at the DIS Robotics Laboratory. The objective of this research is twofold: to develop the hardware and software tools necessary to perform automatic test for paragliders certification and to devise a robotized paraglider able to accomplish long-range delivery or monitoring tasks. The systems considered here are composed by a parafoil and a payload and they can be controlled by means of flap located at the tail of the canopy. Several approaches can be used to describe the dynamics and the aerodynamics of the parafoil. In many works the system is described as a 6 degrees of freedom (DoF) rigid system, including three inertial position components of the system mass center as well as the three Euler orientation angles of the parafoil and payload system [1]. Redelinghuys used a 8 DoF model: six for the air vehicle and two relative rotations for the parafoil, obtained by developing a quasi-Hamiltonian formulation of the equations of motion [2]. The aerodynamic forces and moments acting on the system can be computed using proper coefficients which depend on the canopy (dimension, shape of the profile, etc.). Schroeder Iacomini and Cerimele developed a database for longitudinal and lateral directional aerodynamic, analyzing data collected during several large parafoil drop tests conducted by NASA [3, 4]. The NASA Johnson Space Center built a 4200 ft^2 parafoil for the U.S. Army Natick Soldier Center to demonstrate autonomous flight using a guided parafoil system to deliver 10,000 lbs of useable payload. The parafoil system, simulation results, and the results of the drop tests are described in Stein et al. [5].

The models proposed here are: a 9 DoF model based on Newton-Euler approach, useful for parafoil certification tests, and a 6 DoF model used for planning and control design.

2 A 9 DoF model of a parafoil and payload system

In the model developed in this section, 3 DoF are used to describe the inertial position of the joint point, and three Euler angles for the parafoil and the payload describe their attitude motion. The system is treated as a multibody and reaction forces are exerted at the joint. Reactions are dynamical unknown and have to be determined. Aerodynamic drag and weight act on the payload, while on the parafoil aerodynamic forces (lift, drag, sideslip force) and moments (rolling, pitching, yawing), apparent forces and moments are considered. Moreover a spring damper mechanism at the joint is assumed to model the resistance to twisting of the coupling joint.
In the following the common shorthand notation for trigonometric function is employed, where $\sin \alpha = s_\alpha$, $\cos \alpha = c_\alpha$, $\tan \alpha = t_\alpha$.

2.1 System kinematics

The variables used are the three inertial coordinates of the joint X_c, plus three Euler angles for the canopy and the payload. The kinematic equations can be easily written by integrating the velocity to obtain the position and by determining the derivatives of the Euler angles from the angular velocity ω:

$$\dot{X}_c = V_c$$

$$\begin{bmatrix} \dot{\phi}_b \\ \dot{\theta}_b \\ \dot{\psi}_b \end{bmatrix} = \begin{bmatrix} 1 & s_{\phi_b} t_{\theta_b} & c_{\phi_b} t_{\theta_b} \\ 0 & c_{\phi_b} & -s_{\phi_b} \\ 0 & s_{\phi_b}/c_{\theta_b} & c_{\phi_b}/c_{\theta_b} \end{bmatrix} \omega_b$$

$$\begin{bmatrix} \dot{\phi}_p \\ \dot{\theta}_p \\ \dot{\psi}_p \end{bmatrix} = \begin{bmatrix} 1 & s_{\phi_p} t_{\theta_p} & c_{\phi_p} t_{\theta_p} \\ 0 & c_{\phi_p} & -s_{\phi_p} \\ 0 & s_{\phi_p}/c_{\theta_p} & c_{\phi_p}/c_{\theta_p} \end{bmatrix} \omega_p.$$

The angular velocity ω_b and ω_p are expressed in the payload and parafoil body fixed reference frame, respectively. Position, velocity and acceleration of parafoil and payload are kinematically derived from the data of the joint and the information related to the attitude and the angular velocity of the bodies, as detailed in the following.
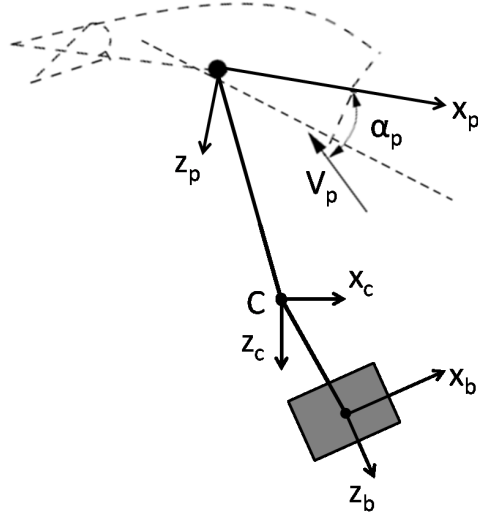
Figure 1: Frames of reference.

2.1.1 Kinematics of the payload

The position of the CG in the body fixed reference frame can be obtained as the sum of the joint's position, properly projected onto the body fixed reference frame, and the relative position between the CG and the joint (which is a constant vector since the body is assumed to be rigid):

$$X_b = T_b X_c + X_{cb}$$

where X_{cb} is the vector from C to the CG of the payload in the body fixed reference frame and T_b is the rotation matrix from inertial to body fixed reference frame

$$T_b = \begin{bmatrix} c_{\theta_b} c_{\psi_b} & c_{\theta_b} s_{\psi_b} & -s_{\theta_b} \\ s_{\phi_b} s_{\theta_b} c_{\psi_b} - c_{\phi_b} s_{\psi_b} & s_{\phi_b} s_{\theta_b} s_{\psi_b} + c_{\phi_b} c_{\psi_b} & s_{\phi_b} c_{\theta_b} \\ c_{\phi_b} s_{\theta_b} c_{\psi_b} + s_{\phi_b} s_{\psi_b} & c_{\phi_b} s_{\theta_b} s_{\psi_b} - s_{\phi_b} c_{\psi_b} & c_{\phi_b} c_{\theta_b}; \end{bmatrix}$$

The velocity is the sum of the traslational and rotational velocity:

$$V_b = T_b V_c + \omega_b \wedge X_{cb} = T_b V_c + \Omega_b X_{cb}$$

being

$$\Omega_b = \begin{bmatrix} 0 & -\omega_b(3) & \omega_b(2) \\ \omega_b(3) & 0 & -\omega_b(1) \\ -\omega_b(2) & \omega_b(1) & 0 \end{bmatrix}$$

Deriving again the acceleration is obtained:

$$a_b = T_b \dot{V}_c + \Omega_b \Omega_b X_{cb} + \dot{\Omega}_b X_{cb} = T_b \dot{V}_c + \Omega_b \Omega_b X_{cb} - R_{cb} \dot{\omega}_b$$

being

$$R_{cb} = \begin{bmatrix} 0 & -X_{cb}(3) & X_{cb}(2) \\ X_{cb}(3) & 0 & -X_{cb}(1) \\ -X_{cb}(2) & X_{cb}(1) & 0 \end{bmatrix}$$

2.1.2 Kinematics of the parafoil

Analogously to what said for the payload, position, velocity and acceleration of the CG of the parafoil are written in the parafoil body fixed reference frame:

$$X_p = T_p X_c + X_{cp}$$

where X_{cp} is the vector from C to the CG of the parafoil in the body fixed reference frame and T_p is the rotation matrix from inertial to body fixed reference frame

$$T_p = \begin{bmatrix} c_{\theta_p} c_{\psi_p} & c_{\theta_p} s_{\psi_p} & -s_{\theta_p} \\ s_{\phi_p} s_{\theta_p} c_{\psi_p} - c_{\phi_p} s_{\psi_p} & s_{\phi_p} s_{\theta_p} s_{\psi_p} + c_{\phi_p} c_{\psi_p} & s_{\phi_p} c_{\theta_p} \\ c_{\phi_p} s_{\theta_p} c_{\psi_p} + s_{\phi_p} s_{\psi_p} & c_{\phi_p} s_{\theta_p} s_{\psi_p} - s_{\phi_p} c_{\psi_p} & c_{\phi_p} c_{\theta_p} \end{bmatrix}.$$

The velocity of the parafoil is:

$$V_p = T_p V_c + \Omega_p X_{cp}$$

and deriving again with respect to the time the acceleration is obtained

$$a_p = T_p \dot{V}_c + \Omega_p \Omega_p X_{cp} - R_{cp} \dot{\omega}_p$$

being

$$\Omega_p = \begin{bmatrix} 0 & -\omega_p(3) & \omega_p(2) \\ \omega_p(3) & 0 & -\omega_p(1) \\ -\omega_p(2) & \omega_p(1) & 0 \end{bmatrix} \quad R_{cp} = \begin{bmatrix} 0 & -X_{cp}(3) & X_{cp}(2) \\ X_{cp}(3) & 0 & -X_{cp}(1) \\ -X_{cp}(2) & X_{cp}(1) & 0 \end{bmatrix}.$$

The acceleration expressed as function of the joint acceleration, the angular acceleration and the angular velocity is used to write the dynamics of the system using a multibody approach.

2.2 System dynamics

2.2.1 Dynamics of the payload

The equation of motion for the payload can be written:

$$M_b a_b = F_A^b + W^b - T_b F_R$$

where F_A^b is the aerodynamic force, W^b is the weight force and F_R is the reaction exerted at the joint, expressed in the inertial reference frame, which are projected onto the body fixed reference frame by means of T_b.
The only aerodynamic force acting on the payload is the drag, which can be computed as

$$F_A^b = -\frac{1}{2} \rho S_b \left| V_b \right| C_D^b \begin{bmatrix} V_b(1) \\ V_b(2) \\ V_b(3) \end{bmatrix} \tag{1}$$

The drag coefficient C_D^b depends on the angle of attack $\alpha_b = \tan^{-1}(V_b(3)/V_b(1))$

$$C_D^b = C_{D_0} + C_{D_\alpha} \alpha_b^2.$$

The weight forces has to be projected onto the body fixed reference frame

$$W^b = m_b g \begin{bmatrix} -s_{\theta_b} \\ s_{\phi_b} c_{\theta_b} \\ c_{\phi_b} c_{\theta_b} \end{bmatrix}.$$

Finally, bringing all the known terms to the right, the equation of motion can be rewritten as:

$$M_b T_b \dot{V}_c - M_b R_{cb} \dot{\omega}_b + T_b F_R = F_A^b + W^b - M_b \Omega_b \Omega_b X_{cb}.$$

4

The balance of moments is

$$I_b \dot{\omega}_b + \omega_b \wedge I_b \omega_b = M_c - X_{bc} \wedge T_b F_R$$
$$I_b \dot{\omega}_b + \Omega_b I_b \omega_b = M_c + R_{cb} T_b F_R$$

where M_c is the resistance to twisting of the coupling joint and $R_{cb}T_b$ is the moment generated on the CG due to the reaction forces.

The resistance to twisting of the coupling joint can be modeled as a spring damper mechanism [6].

$$M_c = \begin{bmatrix} 0 \\ 0 \\ K_c(\tilde{\psi}_p - \tilde{\psi}_b) + C_c(\dot{\tilde{\psi}}_p - \dot{\tilde{\psi}}_b) \end{bmatrix}$$

The angles $\tilde{\psi}_p$ and $\tilde{\psi}_b$ are the modified Euler yaw angles of the parafoil and payload that come from a modified sequence of rotations where the Euler yaw angle is the final rotation. $\tilde{\psi}_p$ and $\tilde{\psi}_b$ and their derivatives can be related to the original Euler angles:

$$\tilde{\psi}_b = \tan^{-1}\left(\frac{s_{\phi_b} s_{\theta_b} c_{\psi_b} - c_{\phi_b} s_{\psi_b}}{c_{\theta_b} c_{\psi_b}}\right) \qquad \dot{\tilde{\psi}}_b = \begin{bmatrix} -c_{\tilde{\theta}_b} t_{\tilde{\theta}_b} & s_{\tilde{\theta}_b} t_{\tilde{\theta}_b} & 1 \end{bmatrix} \omega_b$$

$$\tilde{\psi}_p = \tan^{-1}\left(\frac{s_{\phi_p} s_{\theta_p} c_{\psi_p} - c_{\phi_p} s_{\psi_p}}{c_{\theta_p} c_{\psi_p}}\right) \qquad \dot{\tilde{\psi}}_p = \begin{bmatrix} -c_{\tilde{\theta}_p} t_{\tilde{\theta}_p} & s_{\tilde{\theta}_p} t_{\tilde{\theta}_p} & 1 \end{bmatrix} \omega_p$$

being

$$t_{\tilde{\theta}_b} = \frac{c_{\phi_b} s_{\theta_b} c_{\psi_b} + s_{\phi_b} s_{\psi_b} c_{\tilde{\psi}_b}}{c_{\theta_b} c_{\psi_b}} \qquad t_{\tilde{\theta}_p} = \frac{c_{\phi_p} s_{\theta_p} c_{\psi_p} + s_{\phi_p} s_{\psi_p} c_{\tilde{\psi}_p}}{c_{\theta_p} c_{\psi_p}} \quad .$$

Taking all the known terms to the right, the rotational equation of motion becomes:

$$I_b \dot{\omega}_b - R_{cb} T_b F_R = M_c - \Omega_b I_b \omega_b.$$

2.2.2 Dynamics of the parafoil

The equation of motion for the parafoil can be written as:

$$M_p a_p = F_A^p + F_{app} + W^p - T_p F_R$$

where F_A^p is the aerodynamic force, W^p is the weight force, F_{app} is the vector of apparent forces and $-T_p F_R$ is the projection of the reaction forces, with opposite sign with respect to the reactions acting on the payload, onto the body fixed reference frame.

The aerodynamic force contains lift and drag:

$$F_A^p = \frac{1}{2}\rho S_p |V_p| C_L \begin{bmatrix} V_p(3) \\ 0 \\ -V_p(1) \end{bmatrix} - \frac{1}{2}\rho S_p |V_p| C_D^p \begin{bmatrix} V_p(1) \\ V_p(2) \\ V_p(3) \end{bmatrix}. \tag{2}$$

The lift and drag coefficient C_L and C_D^p depend on the angle of attack $\alpha_p = \tan^{-1}(V_p(3), V_p(1))$.

$$C_L = C_{L_0} + C_{L_\alpha}\alpha_p$$
$$C_D^p = C_{D_0} + C_{D_\alpha}\alpha_p^2$$

The weight forces has to be projected onto the body fixed reference frame

$$W^p = m_p g \begin{bmatrix} -s_{\theta_p} \\ s_{\phi_p} c_{\theta_p} \\ c_{\phi_p} c_{\theta_p} \end{bmatrix}.$$

F_{app} is the vector of apparent force exerted by the fluid on the body: when a body moves in a fluid it sets that fluid in motion thus creating an additional field of fluid momentum and energy surrounding the body.

$$F_{app} = -M_F a_p - \omega_p \wedge M_F \dot{X}_p = -M_F T_p \dot{V}_c - M_F \Omega_p \Omega_p X_{cp} + M_F R_{cp} \dot{\omega}_p - \Omega_p M_F (T_p V_c + \Omega_p X_{cp})$$

The apparent mass M_F can be computed using the formulas given by Lissaman and Brown [7]:

$$M_F = \begin{bmatrix} A & 0 & 0 \\ 0 & B & 0 \\ 0 & 0 & C \end{bmatrix}. \tag{3}$$

The terms A, B, C are computed as follows

$$
\begin{aligned}
k_A &= 0.848\frac{\pi}{4} & A &= k_A \rho t^2 b \left(1 + \frac{8}{3}a^3\right) \\
k_B &= 0.339\frac{\pi}{4} & B &= k_B \rho \left[t^2 + 2a^2(1 - t^2)\right] c \\
k_C &= \frac{AR}{1 + AR}\frac{\pi}{4} & C &= k_C \rho c^2 b \sqrt{1 + 2a^2(1 - t^2)}
\end{aligned}
$$

being $AR = \dfrac{b}{c}$ the aspect ratio and a the high of the arc in the mid point (when the canopy is arching the effective length from the span b to the arc length of the canopy increases).

Finally, bringing all the known terms to the right, the equation of motion is obtained as:

$$(M_p + M_F)T_p \dot{V}_c - (M_p + M_F)R_{cp}\dot{\omega}_p - T_p F_R = F_A^p + W^p - (M_p + M_F)\Omega_p \Omega_p X_{cp} - \Omega_p M_F (T_p X_c + \Omega_p X_{cp}).$$

The balance of moments is

$$I_p \dot{\omega}_p + \Omega_p I_p \omega_p = M_A^p + M_{app} - T_p T_b^T M_c - X_{cp} \wedge T_p F_R$$

where M_A^p is the aerodynamic moment, M_{app} is the moment generated by the apparent forces, $R_{cp}T_b F_R$ is the moment generated on the CG due to the reaction forces.
The aerodynamics generates rolling, pitching and yawing moments:

$$M_A^p = \frac{1}{2}\rho S_p |V_p|^2 \begin{bmatrix} C_{l_p} b^2 \dfrac{\omega_p(1)}{2|V_p|} + C_{l_\phi} b \phi_p \\[2mm] C_{m_q} c^2 \dfrac{\omega_p(2)}{2|V_p|} + C_{m_0} c + C_{m_\alpha} c \alpha_p \\[2mm] C_{n_r} b^2 \dfrac{\omega_p(3)}{2|V_p|} \end{bmatrix}. \tag{4}$$

The vector of apparent moments can be computed as

$$M_{app} = -I_F \dot{\omega}_p - \Omega_p I_F \omega_p - V_p \wedge M_F V_p = -I_F \dot{\omega}_p - \Omega_p I_F \omega_p - \Xi_p M_F V_p \tag{5}$$

being

$$\Xi_p = \begin{bmatrix} 0 & -V_p(3) & V_p(2) \\ V_p(3) & 0 & -V_p(1) \\ -V_p(2) & V_p(1) & 0 \end{bmatrix}.$$

As for the apparent masses, the apparent moment of inertia are computed using the formulas given by Lissaman and Brown [7]:

$$I_F = \begin{bmatrix} I_A & 0 & 0 \\ 0 & I_B & 0 \\ 0 & 0 & I_C \end{bmatrix}.$$

For a planar canopy the terms I_A, I_B, I_C are defined as follows

$$
\begin{aligned}
k_A^* &= 0.055 \frac{AR}{1 + AR} & I_A &= k_A^* \rho c^2 b^3 \\
k_B^* &= 0.0308 \frac{AR}{1 + AR} & I_b &= k_B^* \rho c^4 b \left[1 + \frac{\pi}{6}(1 + AR)ARa^2 t^2 \right] \\
k_C^* &= 0.0555 & I_C &= k_C^* \rho t^2 b^3 \left(1 + 8a^2 \right).
\end{aligned}
$$

As done previously, it follows that

$$
(I_p + I_F)\dot{\omega}_p + R_{cp}T_p F_R = M_A^p - Tp T_b^T M_c - \Omega_p(I_p + I_F)\omega_p - \Xi_p M_F V_p.
$$

2.2.3 Effect of flaps deflection on the aerodynamics

Beside the angle of attack, the aerodynamics coefficients also depend on the flap deflection. The two flaps located at the tail of the parafoil, on the sides, can be deflected only in one direction: if they are both deflected of the same angle, then an increase of lift and drag occur, while the efficiency decreases. If the deflection of the flaps is asymmetric, then there is a variation of the rolling and yawing moments, which make the system turn. Such behavior can be model by introducing the terms symmetrical flaps deflection $\delta_s = \min(\delta_{Left}, \delta_{Right})$ and differential flaps deflection $\delta_a = \delta_{Left} - \delta_{Right}$.

δ_a and δ_s influences both longitudinal and lateral aerodynamics coefficients. The variation of C_L and C_D is always positive, while the moment is positive when the left flap is more deflected than the right and vice versa.

Therefore the variation of the flap determines a variation of aerodynamic forces and moments:

$$
\Delta F_a^p = \frac{1}{2}\rho S_p |V_p| \begin{bmatrix} \left[C_{L_{\delta_a}} V_p(3) - C_{D_{\delta_a}} V_p(1) \right] \text{sign}(\delta_a) & C_{L_{\delta_s}} V_p(3) - C_{D_{\delta_s}} V_p(1) \\ -C_{D_{\delta_a}} V_p(2)\text{sign}(\delta_a) & -C_{D_{\delta_s}} V_p(2) \\ \left[-C_{L_{\delta_a}} V_p(1) - C_{D_{\delta_a}} V_p(3) \right] \text{sign}(\delta_a) & -C_{L_{\delta_s}} V_p(1) - C_{D_{\delta_s}} V_p(3) \end{bmatrix} \begin{bmatrix} \delta_a \\ \delta_s \end{bmatrix} = S_{F_a^p} \begin{bmatrix} \delta_a \\ \delta_s \end{bmatrix}.
\tag{6}
$$

Only the asymmetric flap deflection acts on the moments, producing a rolling and yawing moment variation:

$$
\Delta M_a^p = \frac{1}{2}\rho S_p |V_p|^2 \begin{bmatrix} C_{l_{\delta_a}} b/t & 0 \\ 0 & 0 \\ C_{n_{\delta_a}} b/t & 0 \end{bmatrix} \begin{bmatrix} \delta_a \\ \delta_s \end{bmatrix} = S_{M_a^p} \begin{bmatrix} \delta_a \\ \delta_s \end{bmatrix}.
\tag{7}
$$

2.2.4 Dynamic equations of motion

The dynamics equations derived for the payload and the parafoil can be written in a matrix form as follows:

$$
\begin{bmatrix} (M_p + M_F)T_p & -(M_p + M_F)R_{cp} & 0 & -T_p \\ 0 & I_p + I_F & 0 & R_{cp}T_p \\ M_b T_b & 0 & -M_b R_{cb} & T_b \\ 0 & 0 & I_b & -R_{cb}T_b \end{bmatrix} \begin{bmatrix} \dot{V}_c \\ \dot{\omega}_b \\ \dot{\omega}_p \\ F_R \end{bmatrix} =
$$

$$
\begin{bmatrix} F_A^p + W_p - (M_p + M_F)\Omega_p \Omega_p X_{cp} - \Omega_p M_F(T_p V_c + \Omega_p X_{cp}) \\ M_A^p - T_p T_b^T M_c - \Omega_p(I_p + I_F)\omega_p - \Xi_p M_F V_p \\ F_A^b + W_b - M_b \Omega_b \Omega_b X_{cb} \\ M_c - \Omega_b I_b \omega_b \end{bmatrix} + \begin{bmatrix} S_{F_a^p} \\ S_{M_a^p} \\ 0 \\ 0 \end{bmatrix} \begin{bmatrix} \delta_a \\ \delta_s \end{bmatrix}
$$

which can be rewritten as

$$
A \begin{bmatrix} \dot{V}_c \\ \dot{\omega}_b \\ \dot{\omega}_p \end{bmatrix} = B + S \begin{bmatrix} \delta_a \\ \delta_s \end{bmatrix}.
$$

Finally, inverting the matrix A, it follows that

$$
\begin{bmatrix} \dot{V}_c \\ \dot{\omega}_b \\ \dot{\omega}_p \end{bmatrix} = A^{-1}B + A^{-1}S \begin{bmatrix} \delta_a \\ \delta_s \end{bmatrix} = D + Gu.
$$

2.3 Simulation results

A Matlab code has been developed to simulate the 9 DoF model here described. In Tab. 1 the characteristics of payload and parafoil are reported, while the parafoil and payload aerodynamic coefficients are reported in Tab. 2.

	Payload	Parafoil
Mass [kg]	135	13
Geometry [m]	$0.5 \times 0.5 \times 0.5$	$7 \times 3 \times 0.3$
		[b × c × t]
Surface [m^2]	0.5	21
Distance from joint [m]	0.5	7.5

Table 1: Physical characteristics of the multibody system

C_{L_0}	0.4	C_{L_α}	2
C_{D_0}	0.15	C_{D_α}	1
C_{l_p}	-0.1	C_{l_ϕ}	-0.05
C_{m_q}	-2	C_{m_0}	0.018
C_{n_r}	-0.07	C_{m_α}	-0.2
$C_{L_{\delta_a}}$	0.0001	$C_{L_{\delta_s}}$	0.21
$C_{D_{\delta_a}}$	0.0001	$C_{D_{\delta_s}}$	0.3
$C_{l_{\delta_a}}$	0.0021	$C_{n_{\delta_a}}$	0.004

Table 2: Parafoil and payload aerodynamic coefficients

The moment of inertia of the payload and parafoil are given by the diagonal matrices:

$$I_b = \frac{m_b}{12} \begin{bmatrix} y_b^2 + z_b^2 & 0 & 0 \\ 0 & x_b^2 + z_b^2 & 0 \\ 0 & 0 & x_b^2 + y_b^2 \end{bmatrix} \qquad I_p = \frac{m_p}{12} \begin{bmatrix} b^2 + t^2 & 0 & 0 \\ 0 & c^2 + t^2 & 0 \\ 0 & 0 & b^2 + c^2 \end{bmatrix}.$$

The maneuver simulated is characterized by initial altitude of 5000 m, starting at rest. Initial angular velocities are equal to zero both for payload and parafoil, as well as the Euler angles.
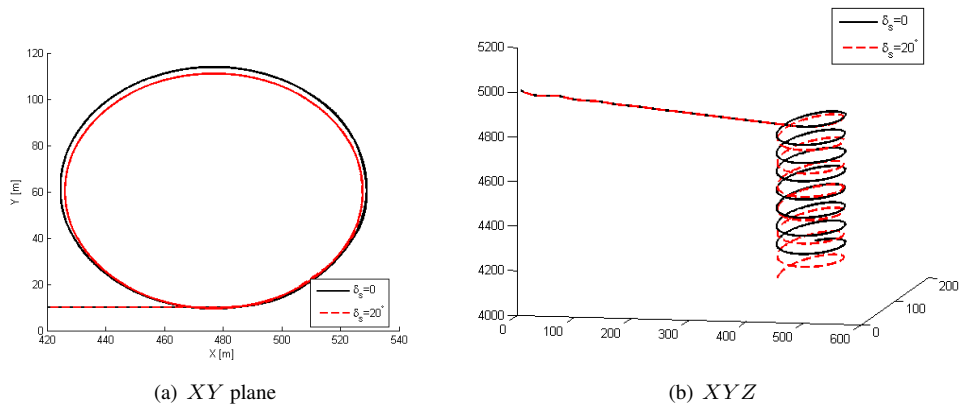
If the system is left in free flight, it glides with a constant glide angle which depends on the geometry and aerodynamic characteristics of the sail. The efficiency, that is the ratio between lift and drag, remains constant. If the flaps are deflected, the glide angle increases since the efficiency of the canopy decrease. Fig. 2(a) shows a comparison between two cases: (i) the flap are never deflected; (ii) the flaps are both deflected of 20° after 50 s. As the flaps are deflected, there is a decrease of the efficiency which goes under a transient and then stabilizes. An increase of the glide angle, which means a higher rate of descent, as flaps deflection is increased is shown in Fig. 2(b), and a variation of the angle of attack with flaps deflection in Fig. 2(c), while the sideslip angle remains equal to zero if the flap variation is symmetric (i.e., $\delta_a = 0$) as shown in Fig. 2(d).

The effect of asymmetric flap deflection is to induce a rolling and, consequently, a yawing moment on the system. If a constant δ_a is commanded the center of mass performs a spiral motion. If together with δ_a a symmetric deflection δ_s is commanded, the system goes down faster while turning. As a consequence the radius of the spiral is smaller. Fig. 3 shows a comparison between the trajectories obtained with $\delta_s = 0$ and $\delta_s = 20°$ ans $\delta_a = +20°$ (the left flap is deflected of 20° while the right flap is in the nominal configuration) after 50 s in both cases.
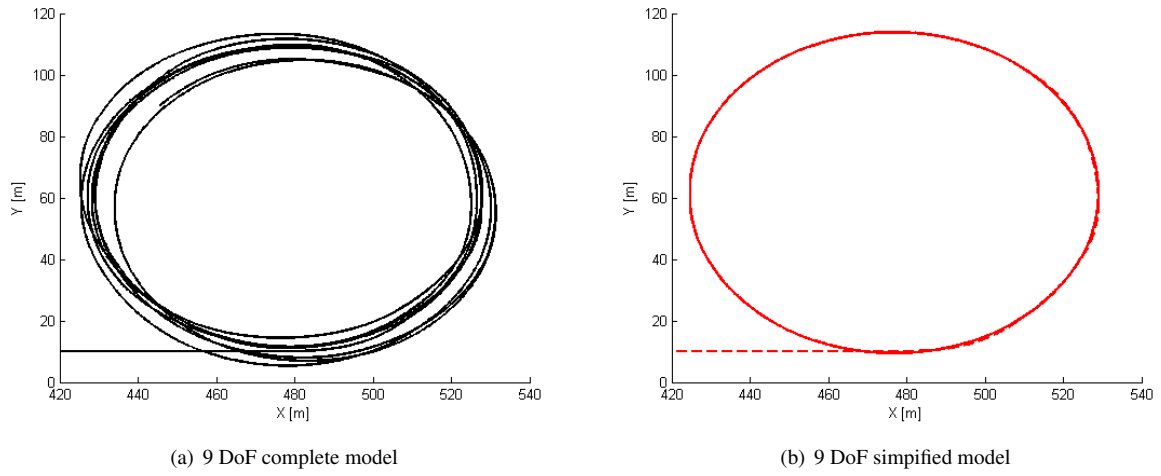
Fig. 4 shows the influence of the payload motion on the path of the center of mass when only $\delta_a = +20°$ is commanded after 50 s. Figure 4(a) reports the XY trajectory of the system when the complete model is considered, while Fig. 4(b) reports the evolution in the XY plane when the torsion exerted at the joint and the drag acting on the payload are neglected. The disturbance induced by the payload on the center of mass motion appears as a drift
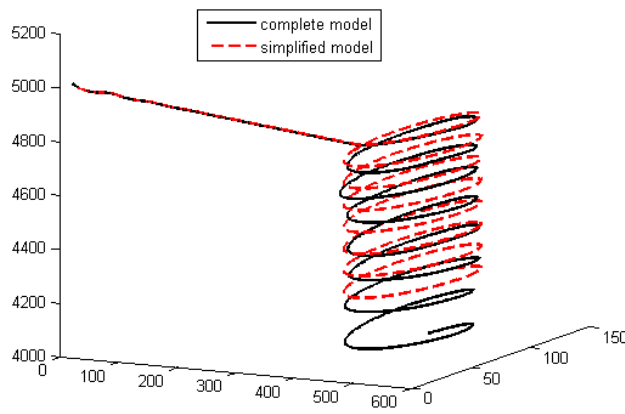
(a) Efficiency

(b) Altitude *vs* Distance

(c) Angle of attack

(d) Sideslip angle
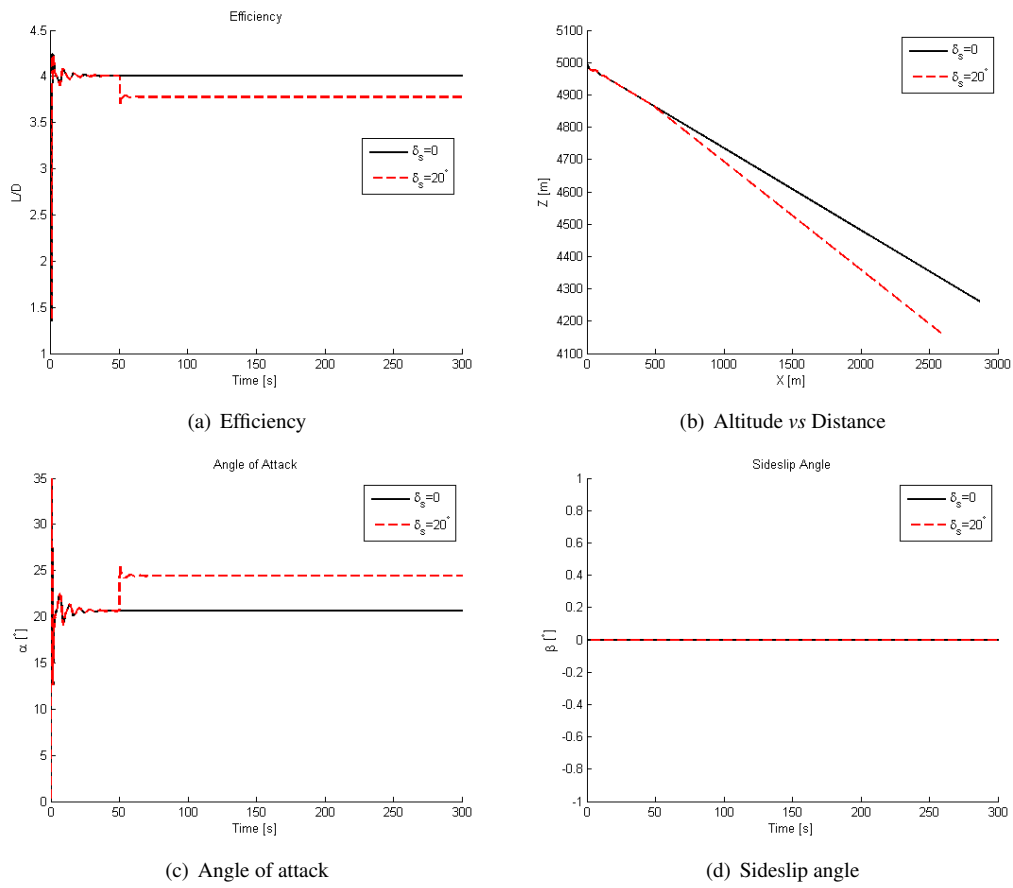
Figure 2: Effects of symmetric flap deflection.

(a) XY plane

(b) XYZ

Figure 3: Trajectory - with and witout δ_s - with $\delta_a = 20°$.

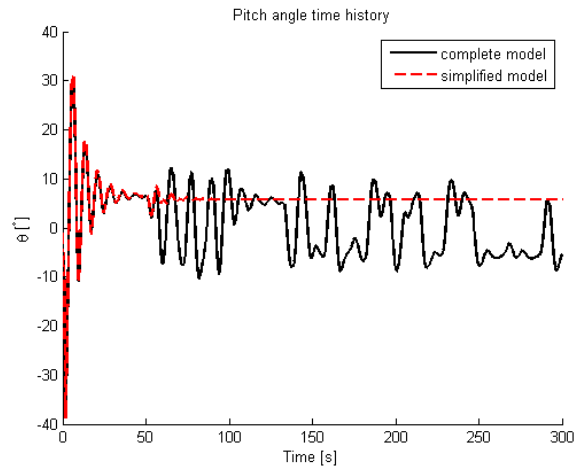9

(a) 9 DoF complete model

(b) 9 DoF simpified model

Figure 4: Effects of the payload twisting: path of the center of mass on the XY plane when δ_a is commanded.
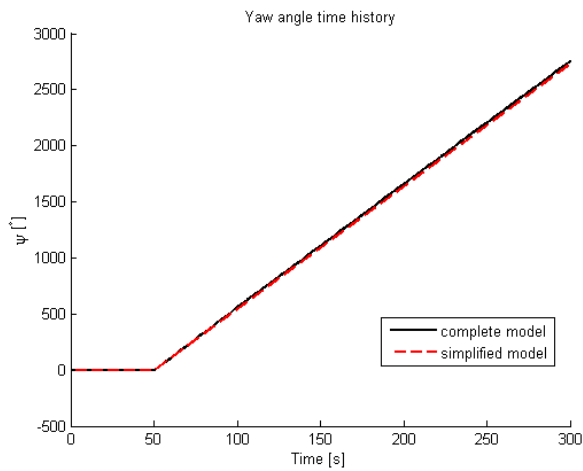

Figure 5: Effects of the payload twisting: 3D path when δ_a is commanded.
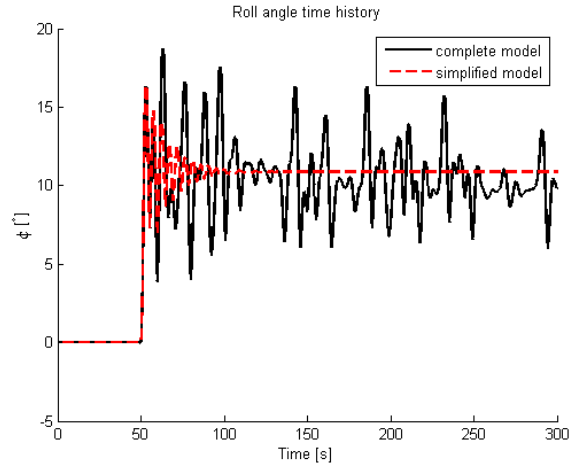
(a) Roll angle ϕ

(b) Pitch angle θ

(c) Yaw angle ψ

Figure 6: Effects of the payload twisting: Attitude variation when δ_a is commanded.

on the XY plane. The influence of the payload twisting on the overall trajectory cannot be determined if a 6 DoF is considered instead.

The motion in the tridimensional space is shown in Fig. 5. The system performs a spiral motion starting at t=50 s. The radius of the spiral depends on the asymmetric flap deflection: as δ_a increases, the radius decreases.

The attitude behavior relative to the spiral motion is shown in Fig. 6. The roll angle has a step variation as the flap are deflected (see Fig. 6(a)), then its value oscillates about an average value. The pitch angle has small oscillations that persist if the complete model is considered (see Fig. 6(b)) when the yaw angle varies with flaps deflection.

3 A 6 DoF model of a parafoil and payload system

3.1 Kinematics

The state vector includes in this case the inertial position of the global center of mass (CM) X_{cm}, the velocity of CM in the body fixed reference frame V_{cm}^b, the Euler angles and the angular velocities.
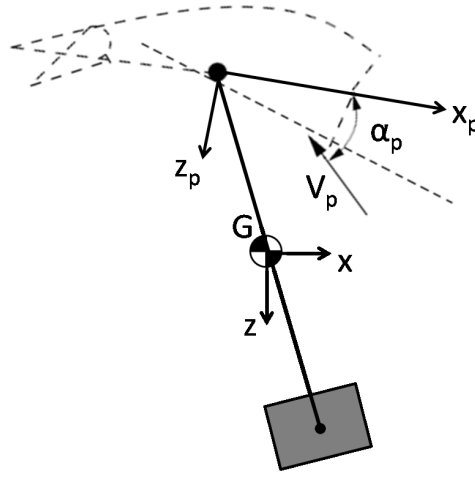

Figure 7: Frames of reference.

The kinematic equations can be easily written by projecting into the inertial reference frame and integrating the velocity to obtain the position and by determining the derivatives of the Euler angles from the angular velocity ω:

$$\dot{X}_{cm} = T_{ib}V_{cm}^b$$

$$\begin{bmatrix} \dot{\phi} \\ \dot{\theta} \\ \dot{\psi} \end{bmatrix} = \begin{bmatrix} 1 & s_\phi t_\theta & c_\phi t_\theta \\ 0 & c_\phi & -s_\phi \\ 0 & s_\phi/c_\theta & c_\phi/c_\theta \end{bmatrix} \omega.$$

The angular velocity ω is expressed in the body fixed reference frame.
The velocity of the payload's center of mass V_b and canopy's center of mass V_p have to be determined in order to compute the aerodynamic forces acting on the system:

$$V_b = V_{cm}^b + \Omega X_{gb}$$
$$V_p = V_{cm}^b + \Omega X_{gp}$$

where

$$\Omega = \begin{bmatrix} 0 & -\omega(3) & \omega(2) \\ \omega(3) & 0 & -\omega(1) \\ -\omega(2) & \omega(1) & 0 \end{bmatrix}$$

12

and X_{gb} and X_{gp} are the vectors from the global to the payload's and canopy's center of mass, repsectively. The acceleration of the center of mass is

$$a_{cm} = \dot{V}_{cm}^b + \omega \wedge V_{cm}^b = \dot{V}_{cm}^b + \Omega V_{cm}^b.$$

3.2 Dynamics

3.2.1 Equilibrium of forces

The equation of motion for the center of mass can be written as:

$$Ma_{cm} = W^b + F_A^p + F_A^b + F_{app}$$

where M is the total mass, W^b is the weight force, F_A^p and F_A^b are the aerodynamic forces acting on the canopy and the payload, respectively, F_{app} is the vector of apparent forces.

The weight forces has to be projected onto the body fixed reference frame

$$W^b = (m_b + m_p)g \begin{bmatrix} -s_\theta \\ s_\phi c_\theta \\ c_\phi c_\theta \end{bmatrix}.$$

The aerodynamic forces F_A^b and F_A^p acting on the payload and on the canopy can be computed respectively as in (1) and (2).

F_{app} is the vector of apparent force exerted by the fluid on the body:

$$F_{app} = -M_F a - \omega \wedge M_F V_p = -M_F a - \Omega M_F V_p.$$

The apparent mass M_F can be computed as in (3).

Rearranging, the equation of motion becomes

$$(M + M_F)\dot{V}_{cm}^b = W^b + F_A^p + F_A^b - \Omega M_F V_p - (M + M_F)\Omega V_{cm}^b.$$

3.2.2 Balance of moments

The balance of moments about the center of mass is

$$I\dot{\omega} + \Omega I \omega = M_A^p + M_{app} + X_{gp} \wedge F_A^p + X_{gp} \wedge F_{app} + X_{gb} \wedge F_A^b$$

where M_A^p is the aerodynamic moment, M_{app} is the moment generated by the apparent forces, $X_{gp} \wedge F_A^p$, $X_{gp} \wedge F_{app}$ and $X_{gb} \wedge F_A^b$ are the moments generated on the center of mass due to the aerodynamics and apparent forces. It is worth noting that

$$X_{gp} \wedge F_A^p = R_{gp} F_A^p$$

being

$$R_{gp} = \begin{bmatrix} 0 & -X_{gp}(3) & X_{gp}(2) \\ X_{gp}(3) & 0 & -X_{gp}(1) \\ -X_{gp}(2) & X_{gp}(1) & 0 \end{bmatrix}$$

Analogously for $X_{gp} \wedge F_{app} = -R_{gp}M_F\dot{V}_{cm}^b - R_{gp}\Omega M_F V_p$ and $X_{gb} \wedge F_A^b = R_{gb}F_A^b$.

The aerodynamics generates rolling, pitching and yawing moments M_A^p given by (4). The vector of apparent moments M_{app} is computed as in (5).

Finally, it follows that

$$R_{gp}M_F\dot{V}_{cm}^b + (I + I_F)\dot{\omega} = M_A^p - \Xi_p M_F V_p + R_{gp}F_A^p - R_{gp}\Omega M_F V_p + R_{gb}F_A^b - \Omega(I + I_F)\omega.$$

3.2.3 Dynamic equations of motion

The dynamics equations derived for the payload and the parafoil can be written in a matrix form as follows:

$$
\begin{bmatrix} M + M_F & 0 \\ R_{gp}M_F & I + I_F \end{bmatrix} \begin{bmatrix} \dot{V}_{cm}^b \\ \dot{\omega} \end{bmatrix} = \begin{bmatrix} W^b + F_A^p + F_A^b - \Omega M_F V_p - (M + M_F)\Omega V_{cm}^b \\ M_A^p - \Xi_p M_F V_p + R_{gp}F_A^p - R_{gp}\Omega M_F V_p + R_{gb}F_A^b - \Omega(I + I_F)\omega \end{bmatrix} +
$$
$$
+ \begin{bmatrix} S_{F_a^p} \\ S_{M_a^p} + R_{gp}S_{F_a^p} \end{bmatrix} \begin{bmatrix} \delta_a \\ \delta_s \end{bmatrix}
$$

where $S_{F_a^p}$ and $S_{M_a^p}$ are given respectively by eq. (6) and eq. (7).

The above equation can also be written as

$$
A \begin{bmatrix} \dot{V}_{cm}^b \\ \dot{\omega} \end{bmatrix} = B + S \begin{bmatrix} \delta_a \\ \delta_s \end{bmatrix}
$$

and, by inverting the matrix A, it follows

$$
\begin{bmatrix} \dot{V}_{cm}^b \\ \dot{\omega} \end{bmatrix} = D + Gu
$$

being

$$
\begin{aligned}
D &= A^{-1}B \\
G &= A^{-1} \begin{bmatrix} S_{F_a^p} & S_{M_a^p} + R_{gp}S_{F_a^p} \end{bmatrix}^T.
\end{aligned}
$$

4 9 DoF vs 6 DoF model

In this section we analyze the different behavior of the two models developed in the previous sections by comparing the trajectories obtained both on steady state trajectories and in performing agile maneuvers (e.g. the maneuvers prescribed for certification tests). This analysis will be used in deriving the simplified model of the next section.

4.1 Free dynamics

When none of the two flaps is deflected, the 3D system cartesian path is a straight line for both the 9 DoF and 6 DoF model if no resistance to twisting is induced between the parafoil and the payload. Figure 8 shows a comparison between the cartesian path of a complete 9 DoF model with an initial relative yaw between the parafoil and payload equal to $10°$ and a 6 DoF model with initial yaw angle equal to $10°$. The "drift" from the straight line occurring for the 9 DoF case is due to the resistance to twisting at the joint between parafoil and payload induced by the initial relative yaw (see also Fig. 9(c)). The effect of the resistance force at the joint can also be appreciated by looking at Fig. 9(a) and Fig. 9(b): the convergence of roll and pitch angles to the steady state values is much more noisy for the 9 DoF model.
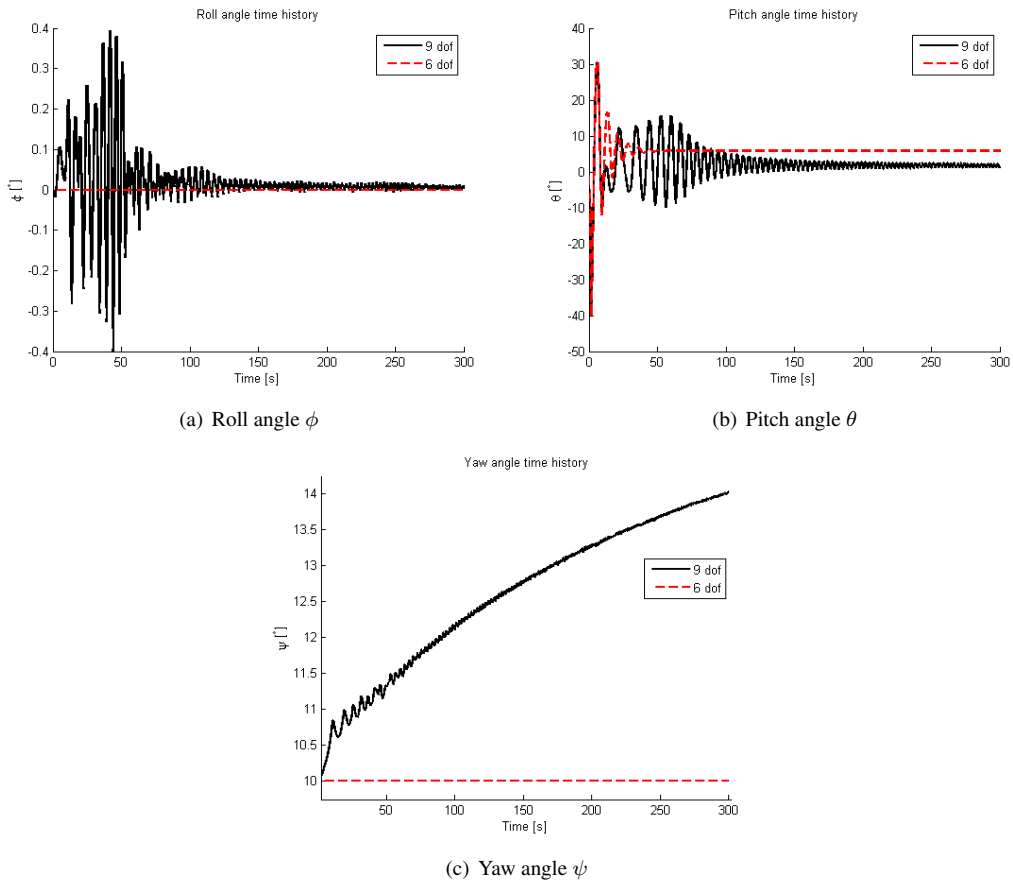
4.2 Spiral

A spiral motion is obtained by applying a constant δ_a. Figure 10 shows the path of the system starting at rest with no deflection of the flaps for 50 s after which a $\delta_a = 20°$ is applied. The projection on the XY plane shows how the two models have a different transient behavior. The 6 DoF model presents a delay in turning and converging to the spiral motion. The behavior is very different at steady state as well, since the 6 DoF model does not present any payload influence resulting in a periodic cartesian motion. The influence of the twisting couple at the joint on the the 9 DoF model produces a drift on the XY plane projection.

4.3 Roll perturbation

The response of the system to an impulsive command of δ_a is an important parameter in sail certification tests. As in the previous cases, Fig. 12 and Fig. 13 show how the disturbance due to the payload motion induces a drift in the yaw angle (see Fig. 13(c)) resulting in a cartesian path different from that of the 6 DoF case.
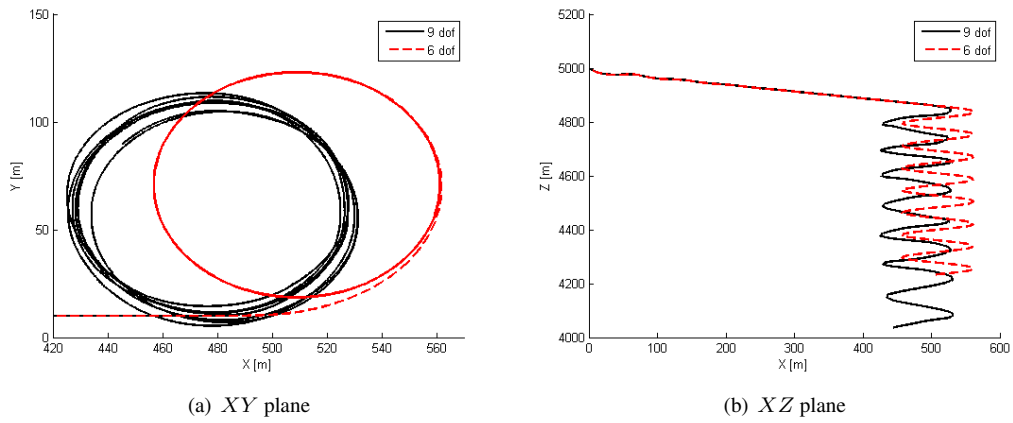
(a) XY plane

(b) XZ plane
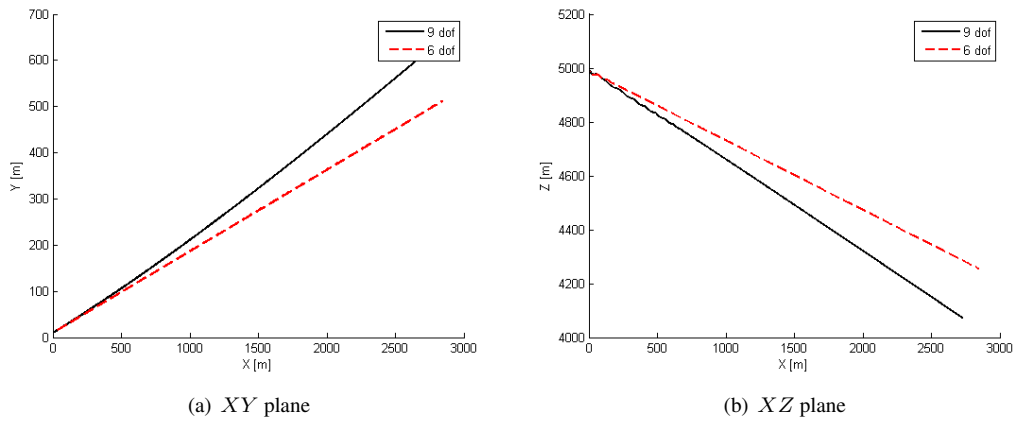
Figure 8: 9 DoF vs 6 DoF: 3D cartesian path in the absence of flaps deflection.

(a) Roll angle ϕ

(b) Pitch angle θ

(c) Yaw angle ψ

Figure 9: 9 DoF vs 6 DoF: Attitude variation in the absence of flaps deflection.

15

(a) XY plane

(b) XZ plane

Figure 10: 9 DoF vs 6 DoF: 3D cartesian path for spiral motion.

(a) Roll angle ϕ

(b) Pitch angle θ

(c) Yaw angle ψ
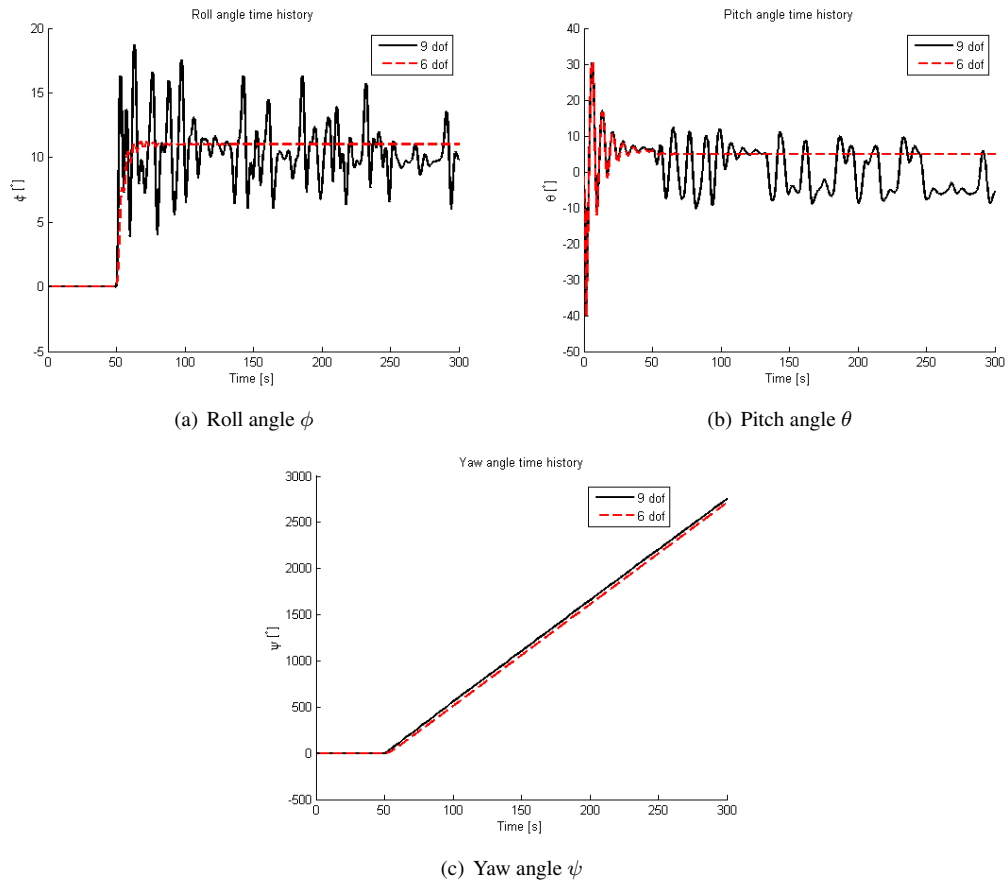
Figure 11: 9 DoF vs 6 DoF: Attitude variation for spiral motion.

(a) XY plane

(b) XZ plane
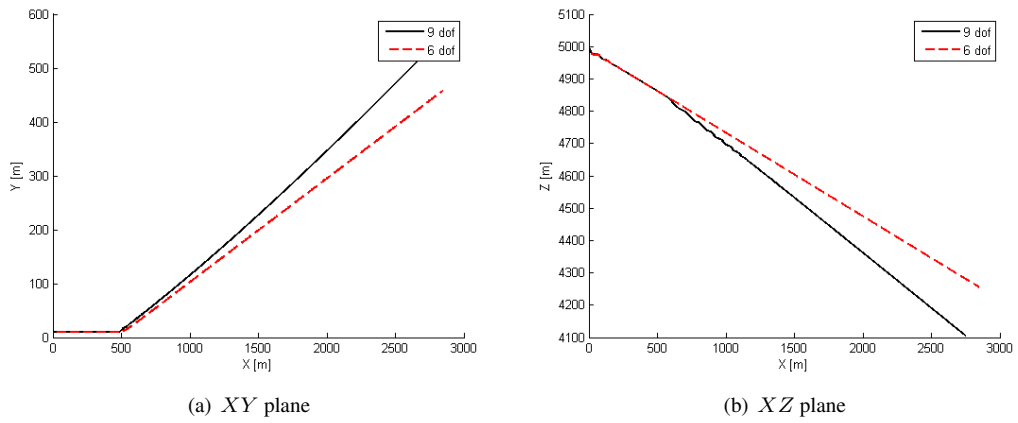
Figure 12: 9 DoF vs 6 DoF: 3D cartesian path when an impulse of δ_a is commanded.

(a) Roll angle ϕ

(b) Pitch angle θ

(c) Yaw angle ψ
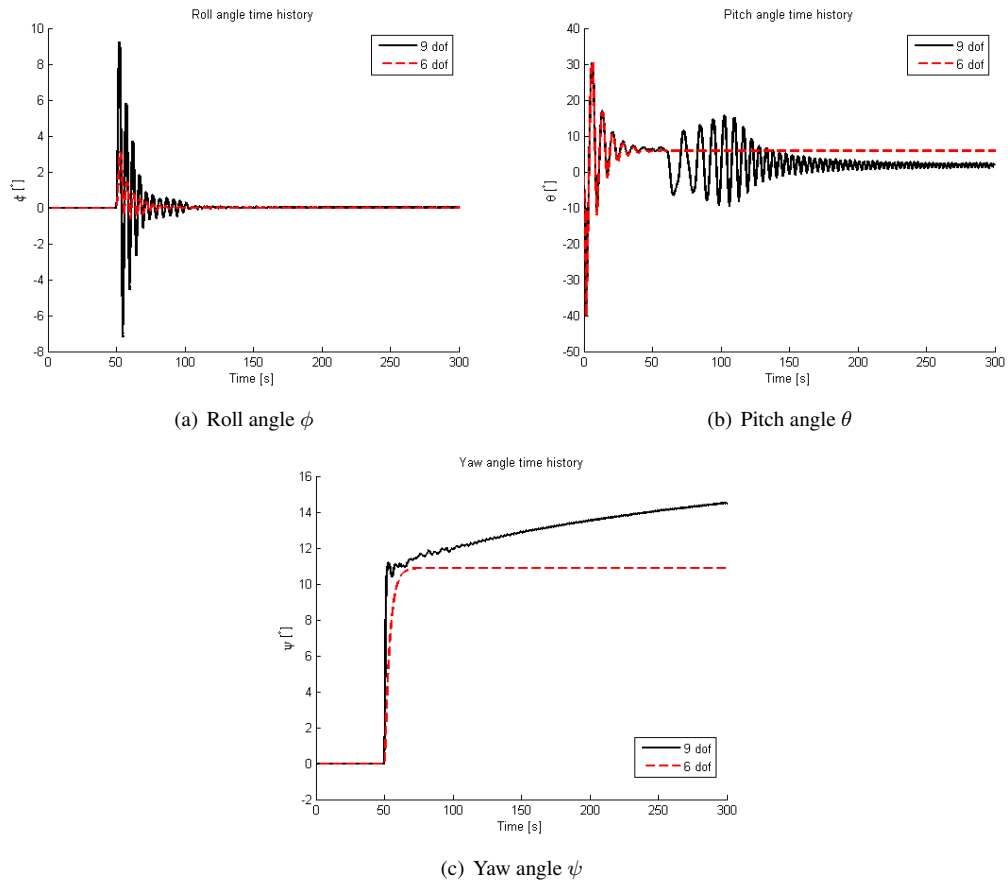
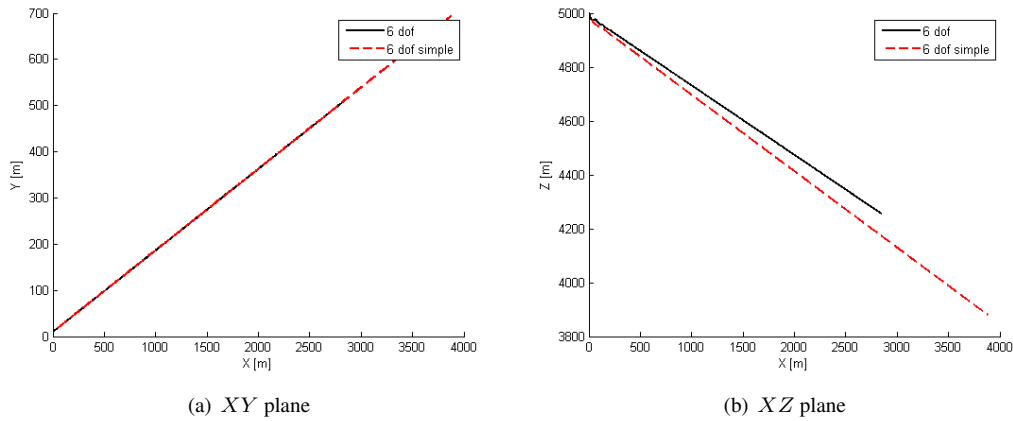**Figure 13:** 9 DoF vs 6 DoF: Attitude variation when an impulse of δ_a is commanded.

5 A simplified 6 DoF model

For the pourpose of control design we have simplified the dynamics of the 6 DoF model by assuming that: (i) apparent mass and inertia effects are negligible; (ii) moments of aerodynamic forces on the center of mass are negligible.
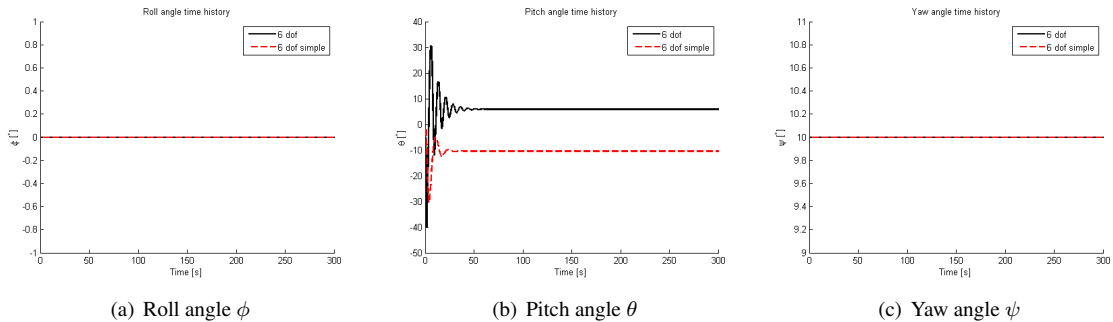
The resulting dynamics is

$$
\begin{aligned}
M\dot{V}_{cm}^b &= W^b + F_A^p + F_A^b - M\Omega V_{cm}^b \\
I\dot{\omega} &= M_A^p - \Omega I\omega.
\end{aligned}
$$

Figures 14–17 report a comparison with the 6 DoF complete model in the case of free dynamics and of spiral motion.

(a) XY plane

(b) XZ plane

Figure 14: 6 DoF vs 6 DoF simplified: 3D cartesian path in the absence of flap deflection.

(a) Roll angle ϕ

(b) Pitch angle θ

(c) Yaw angle ψ

Figure 15: 6 DoF vs 6 DoF simplified: Attitude variation in the absence of flap deflection.

(a) XY plane

(b) XZ plane
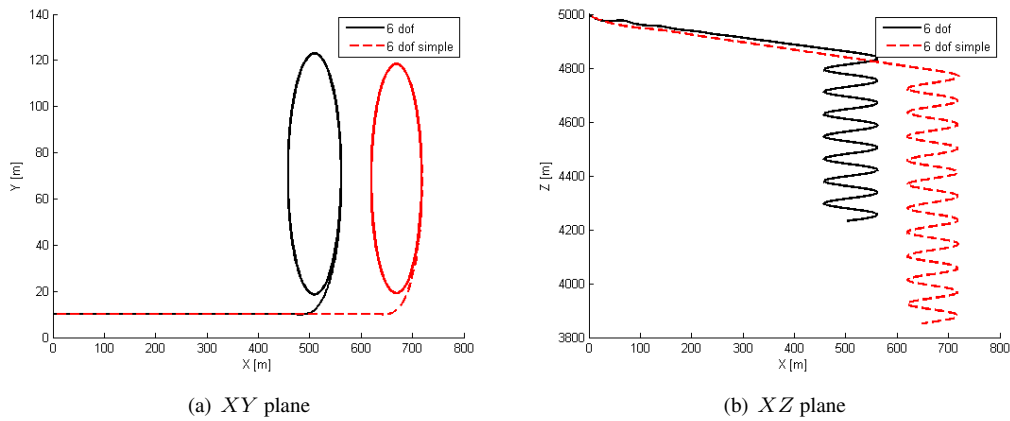
Figure 16: 6 DoF vs 6 DoF simplified: 3D cartesian path for spiral motion.

(a) Roll angle ϕ
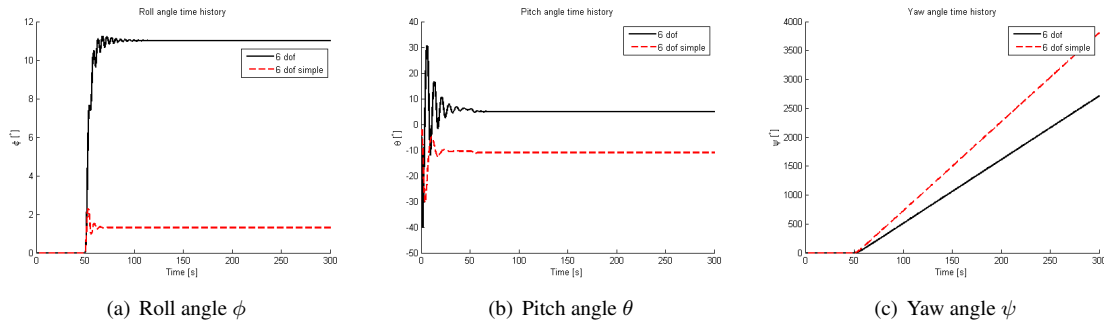
(b) Pitch angle θ

(c) Yaw angle ψ

Figure 17: 6 DoF vs 6 DoF simplified: Attitude variation for spiral motion.

6   Conclusion

In this report we have derived three models of a parafoil and payload system developed with the objective of devising tool useful for sail certification and for the development of autonomous paragliders able to perform long-distance missions. In view of the different problems to be faced in future work, we gradually reduced the complexity of the models while keeping the main motion characteristics of the complete model. This preliminary study led to the design and analysis of the line tracking controller developed in [8].

7   Acknowledgment

References

[1] N. Slegers and M. Costello , *Model Predictive Control of a Parafoil and Payload System*, Journal of Guidance, Control and Dynamics, Vol. 28, No. 4, 2005

[2] C. Redelinghuys, *A Flight Simulation Algorithm for a Parafoil Suspending an Air Vehicle* , Journal of Guidance, Control and Dynamics, Vol. 30, No. 3, 2007

[3] C. Schroeder Iacomini and C.J. Cerimele, *Lateral-Directional Aerodynamics from a Loarge Scale Parafoil Test Program*, AIAA-99-1731, 1999.

[4] C. Schroeder Iacomini and C.J. Cerimele, *Longitudinal Aerodynamics from a Loarge Scale Parafoil Test Program*, AIAA-99-1732, 1999.

[5] J.M. Stein, C.M. Madsen, and A.L. Strahan,*An Overview of the Guided Parafoil System Derived from X-38 Experience*, AIAA-99-1704, 1999.

[6] N. Slegers and M. Costello , *Aspects of Control for a Parafoil and Payload System*, Journal of Guidance, Control and Dynamics, Vol. 26, No. 6, 2003

[7] P.B.S. Lissaman and G.J. Brown, *Apparent Mass Effects on Parafoil Dynamics*, AIAA-93-1236, 1993.

[8] C. Toglia, M. Vendittelli, *Stability analysis of a line tracking algorithm for an autonomous paraglider*, to be submitted to the 49th IEEE Conference on Decision and Control, Atlanta, USA, December 2010.